Pattern formation of an epithelial tubule by mechanical instability during epididymal development.

AUTHOR(S):

Hirashima, Tsuyoshi

CITATION:

Hirashima, Tsuyoshi. Pattern formation of an epithelial tubule by mechanical instability during epididymal development.. Cell reports 2014, 9(3): 866-873

ISSUE DATE:

2014-11-06

URL:

http://hdl.handle.net/2433/193276

Report

Cell Reports

Pattern Formation of an Epithelial Tubule by Mechanical Instability during Epididymal Development

Graphical Abstract

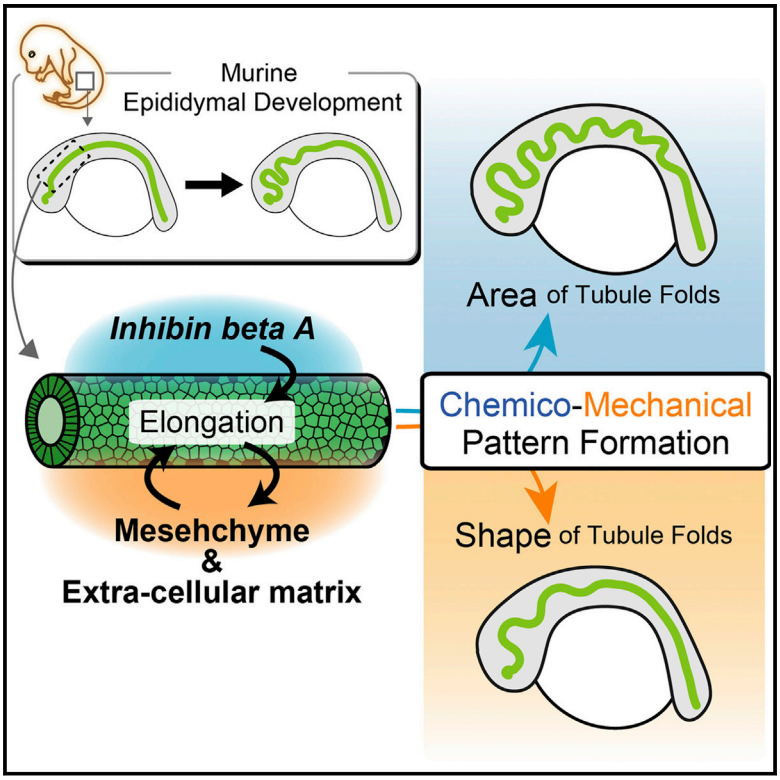

Highlights

Folds in the murine epididymal tubule are formed through a mechanical process

Axial buckling triggered by cell proliferation drives the tubule folding

Cell proliferation area controls where tubule folding occurs

Resistance in tissues surrounding the tubule determines tubule shape

Authors

Tsuyoshi Hirashima

Correspondence

hirashima@frontier.kyoto-u.ac.jp

In Brief

Epithelial tubule shape formation during organ development has been extensively studied from a molecular angle; however, understanding of the mechanical process regulating tubule pattern formation is far from complete. Hirashima finds that murine epididymal tubule shape is determined through mechanical interaction between the developing tubule and its surrounding tissue.

Hirashima, 2014, Cell Reports 9, 866–873
November 6, 2014 ©2014 The Authors
http://dx.doi.org/10.1016/j.celrep.2014.09.041

Cell Reports
Report

Pattern Formation of an Epithelial Tubule by Mechanical Instability during Epididymal Development

Tsuyoshi Hirashima[1,2,*]
[1]Institute for Frontier Medical Sciences, Kyoto University, Kyoto 606-8507, Japan
[2]Institute for Virus Research, Kyoto University, Kyoto 606-8507, Japan
*Correspondence: hirashima@frontier.kyoto-u.ac.jp
http://dx.doi.org/10.1016/j.celrep.2014.09.041

SUMMARY

A single epithelial tubule undergoes morphogenesis to form a functional shape during the development of internal organs; however, the mechanical processes that are directed by the molecular signals regulating tubular morphogenesis are poorly understood. Here, axial tubular buckling triggered by cell proliferation is shown to drive the morphogenesis of murine epididymal tubules through mechanical interactions between the developing epithelial tubule and its surrounding tissues. Through immunofluorescence labeling and mathematical modeling, epididymal tubule shape formation is found to depend on two factors: cell proliferation area in the tubule and mechanical resistance from the tissues surrounding the tubule. Moreover, experimental perturbations of these two factors alter the shape of the epididymal tubule as predicted by the mathematical model, suggesting that the shape of the epididymal tubule spontaneously emerges through mechanical coupling between developing tissues instead of by growing according to a predetermined fate.

INTRODUCTION

During the development of many internal organs, a single epithelial tubule undergoes repetitive deformation and generates a complex but well-organized pattern, such as tree-like branching or coiling, and it has been shown that tubular patterning processes are remarkably stereotypical and reproducible (Joseph et al., 2009; Metzger et al., 2008; Savin et al., 2011). Recent studies have clarified that the morphogenetic processes controlling tubular patterning emerge from both chemical (genes and proteins) and mechanical (stress and strain) interactions between epithelial tissue and surrounding tissues, which contain mesenchyme and extracellular matrix (ECM) (Dong et al., 2014; Savin et al., 2011; Shyer et al., 2013). To elucidate this organogenetic system that generates reproducible morphogenesis, current biomolecular knowledge is used to better understand how mechanical coupling between developing tissues affects tubular patterning.

Tubular pattern formation can be observed during epididymal development in mammalian species wherein the patterning of epididymal tubules begins with local bending and looping in the head region, which is followed by further tubule winding on a plane in the tail region (Joseph et al., 2009; Robaire et al., 2006) (Figure 1A). To elucidate the morphogenetic mechanism of tubule folding, murine genetic experiments have been conducted that illustrate the molecules that are required for normal epididymal development. For example, it has been reported that homozygous inhibin beta A (*Inhba*) knockout mice show a complete absence of the typical folding structure of the epididymal tubule (Tomaszewski et al., 2007). *Inhba* is a member of the transforming growth factor β (TGF-β) family, which is known to form either activins or inhibins via dimerization, and these products then act on the epithelial cells in the epididymal tubule (Ball and Risbridger, 2001; Tomaszewski et al., 2007). The knockout phenotype suggests that the Inhba dimers function as paracrine signals, and TGF-β signaling triggered by *Inhba* provides spatial information related to the future sites of epididymal tubule folding. In addition to providing area specification, one scenario is that the paracrine signals strictly determine the specific region where epididymal tubule bending will occur before it begins; that is, the morphological changes in the epididymal tubule obey predetermined "bend/do not bend" signals at regular intervals (Joseph et al., 2009). Another scenario is that the shape of the tubule, or its wavelength and amplitude, may be spontaneously determined through mechanical interactions during the developmental process.

To clarify the mechanism for achieving the epididymal shape, I study the early process of epididymal morphogenesis related to the tubule folding locally in the head region. By performing the integrative analysis of experiments and modeling, I demonstrate that the shape of the epididymal tubule forms through mechanical interactions between the developing epididymal tubule and surrounding tissues during development.

RESULTS

Morphological Change

During murine development, a simple epididymal tubule undergoes a stereotyped morphogenesis in 3D space and produces

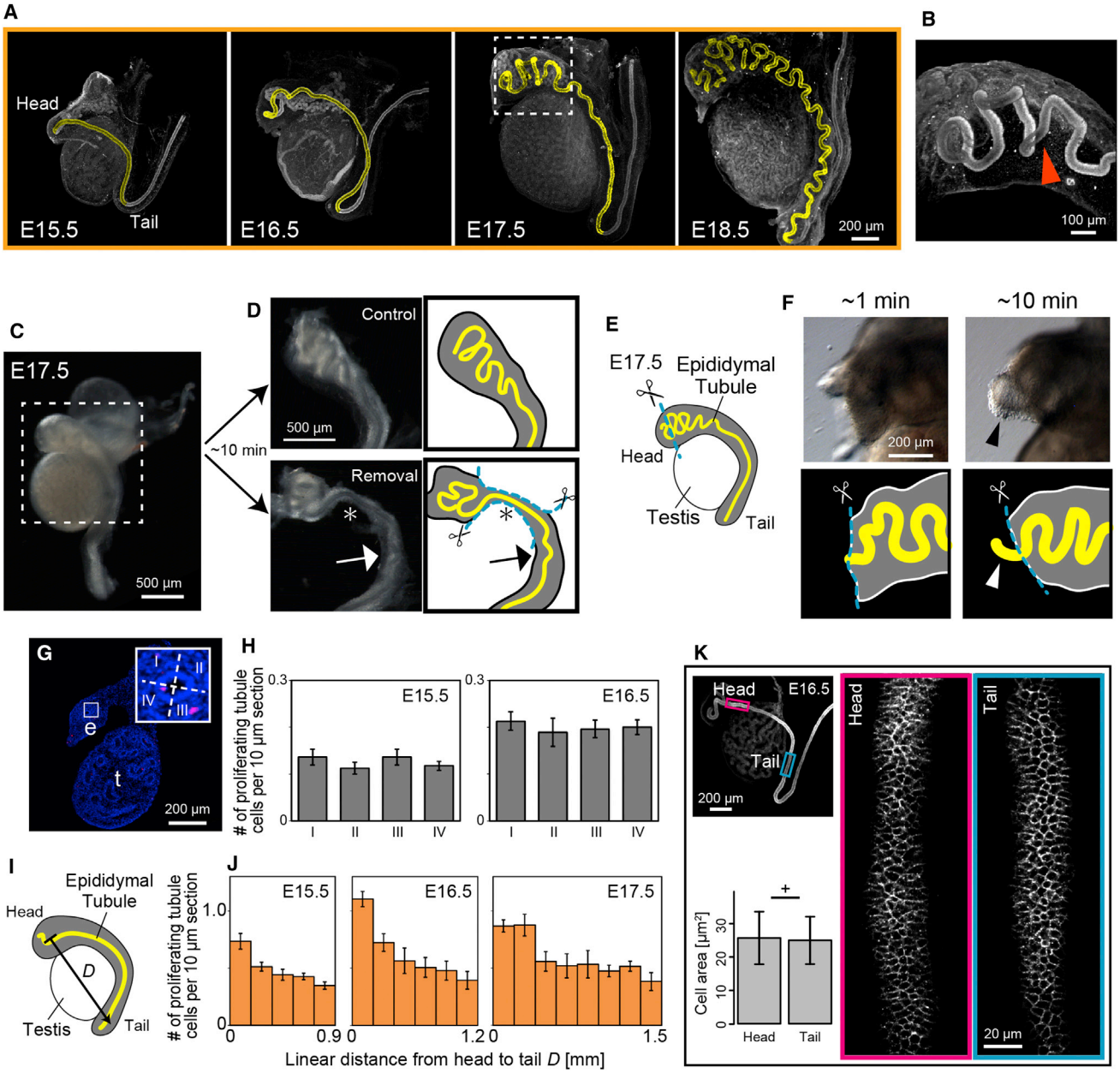

Figure 1. Morphogenesis of the Epididymal Tubule

(A) Morphogenetic development of the epididymal tubule from E15.5 to E18.5. Whole-mount epididymides with testes that were immunostained for Pax2; the manually extracted epididymal tubule is indicated in yellow. Scale bar, 200 μm.

(B) 3D view of the dotted square in (A). The arrowhead represents the point where the handedness of the helix of the tubule changes. Scale bar, 100 μm.

(C–F) Surgical tissue ablation. (C and D) Tissues surrounding the epididymal tubule that were surgically removed. The dotted square represents the area in (D). (D) Left panel shows the epididymis 10 min after the operation, and a drawing is provided in the right panel for clarity. Asterisks specify the removed area, and arrows indicate the area that was not operated on. Scale bar, 500 μm. (E) Schematic representation of the amputation experiment in the distal head region of an epididymis. (F) The lower panel shows a drawing of the image in the upper panel that demonstrates the behavior of the epididymal tubule. The arrowheads indicate where the epididymal tubule protruded from the cutting line. Scale bar, 200 μm.

(G–K) Cellular events. (G) Cross-section of an epididymis stained with DAPI (blue) and immunostained for pHH3 (red). The epididymal tubule is divided into four regions. e, epididymal tubule; t, testis. Scale bar, 200 μm. (H) Schematic diagram shows the distance along the straight line from the head to tail is represented as *D*. (I) Spatial distribution of pHH3-positive cells counted throughout the tubule in the four regions. n = 7. p = 0.46 for E15.5 and 0.76 for E16.5 (Kruskal-Wallis test). (J) Spatial distribution of pHH3-positive cells in the tubule along the linear distance *D*. n = 7. (K) Comparison of cell size and shape in the tubule between the head and tail regions. The cellular membranes were detected by immunostaining for E-cadherin at E16.5. The mean cell area was quantified in the head and tail regions. Scale bars, 200 μm and 20 μm. n = 500. p = 0.24 (Mann-Whitney U test). The error bars represent the SD.

a highly convoluted structure during embryogenesis from embryonic day 15.5 (E15.5) to E18.5 (Figures 1A and S1A). The length of the epididymal tubule elongates past the capsule of the epididymis, the physical border of epididymis, and the folds of the tubule are formed in the head region at the beginning stages of morphogenesis (Figure S1B). Although these morphogenetic changes are highly dynamic, the tubule maintains its single-layered structure, and the diameter is only slightly altered (Figures S1C and S1D).

Close observation of the tubule's shape can reveal how such a stereotyped structure is achieved. When tubule bending begins in the head region, the tubule's deformation is almost planar (Movie S1). Moreover, a 3D view of the folded tubule at a later stage shows that there is at least one point at which the handedness of the helix of the epididymal tubule changes (Figure 1B; Movie S2). These observations revealing two representative shapes clearly exclude the possibility of unidirectional twist-driven tubule patterning, because if tubule twisting were the primary force responsible for this deformation, the resulting shapes should be volumetrically deformed with a biased chirality.

Mechanical Interaction

To examine how the folded tubule mechanically interacts with other tissues in the epididymis, I performed two surgical ablation experiments. First, I detached the epididymis from the testis at E17.5 and carefully removed the surrounding tissues from the epididymal tubule without damaging the tubule (Figure 1C). When the surrounding tissues were removed, the folded structure disappeared, and the tubule became relatively straight within 10 min after the operation; however, the untreated control epididymis maintained the folded tubule shape (n = 5/5; Figure 1D). Note that the tubule folds remained in an area in which the surrounding tissues were attached (Figure 1D, arrow). This experiment suggests that the tubule returns to its original straight shape when external forces are removed. Next, I removed the distal end of the epididymal head region and observed that the shape of the epididymal tubule changed over time (Figure 1E). Surprisingly, the tubule gradually protruded from the cutting line after approximately 10 min, although a significant protrusion was not observed within the first several minutes (n = 7/11; Figure 1F), indicating that the folded tubule is physically confined by the epididymal capsule on the head-tail axis. Note that the observed stress relaxation of the epididymal tubule in these two experiments occurred over a time scale within which cell proliferation does not contribute to tubule deformation. Taken together, the ablation experiments revealed that the folded tubule structure is mechanically supported by the surrounding tissues rather than by self-sustained folding.

Quantification of Cellular Events

To investigate the cellular events that contribute to tubular morphogenesis, I examined the spatial distribution of proliferating cells in the tubule by immunostaining to detect phosphohistone H3 (pHH3) on a plane perpendicular to the head-tail axis *D* (Figure 1I), and I then performed a count of the number of pHH3-positive cells along the axis in the four divided regions (Figure 1G) at E15.5 and E16.5. As shown in Figure 1H, cell proliferation in the tubule occurs almost homogeneously around the circumference of the tubule, suggesting that cell proliferation directly contributes to tubule elongation along the head-tail axis because the tubule's diameter does not change during morphogenesis.

Based on these observations and measurements, an essential mechanism for the formation of tubule folding is proposed as follows. A simple epididymal tubule elongates in a longitudinal direction without intrinsic twisting. At a certain point, the length of the tubule exceeds that of the capsule of the epididymis and generates axial compression in the tubule via mechanical interactions with the epididymal capsule, which leads to structural destabilization, i.e., tubule buckling. Thus, the regular pattern of tubule folds emerges because of mechanical instability.

Next, I attempted to determine how the localized buckling of the epididymal tubule in the head region is achieved by examining the spatial distribution of pHH3-positive cells in the tubule along its linear length *D* (Figures S1E–S1J), and I found that the number of proliferating tubule cells was greater in the head region than in the tail region (Figure 1J). This quantitative result suggests that the elongation rate of the epididymal tubule in the head region is significantly greater than in the tail region as a result of locally enhanced cell proliferation (LECP) in the head region. Additionally, the localization of *Inhba* mRNA expression corroborates the theory of LECP in the head region and ensures differential elongation of the epididymal tubule (Figure S1K). Because there were no significant differences between the head and tail regions in either individual cell size or shape, the localized buckling of the epididymal tubule is presumably independent of individual cellular geometry (Figure 1K).

Mathematical Modeling and Prediction

Although the area of LECP appears to be consistent with the area of localized buckling in the epididymal tubule, it is unclear whether this LECP is sufficient to generate the localized buckling of the epididymal tubule. To address this issue, I considered a system in which an epididymal tubule is embedded into surrounding tissue types, including mesenchyme and ECM, and covered by the cylinder-shaped capsule of the epididymis (Figure 2A), and I devised a mathematical model that can mimic the dynamics of the epididymal tubule (Figure S2; Supplemental Experimental Procedures; Golubovic et al., 2000; Wada and Netz, 2009).

To quantify the shape of the epididymal tubule that is produced by the model and compare the model results with observations, I used the following four morphometric quantities: wavelength of the folded tubule (λ), degree of fold localization (ϕ), average vertical length of the folded tubule (*V*), and average radius of the folded tubule (*R*) (Figure 2B; Supplemental Experimental Procedures). Based on either the measured or properly estimated parameter values, I performed a numerical simulation of the model and confirmed that it is capable of faithfully reproducing the observed pattern by comparing the defined morphometric quantities of the morphology produced in silico with that of the morphology observed in vivo (Figures S2C–S2E; Movie S3; Table S1).

To examine how altering the model parameters influences the shape of the epididymal tubule, I performed extensive numerical

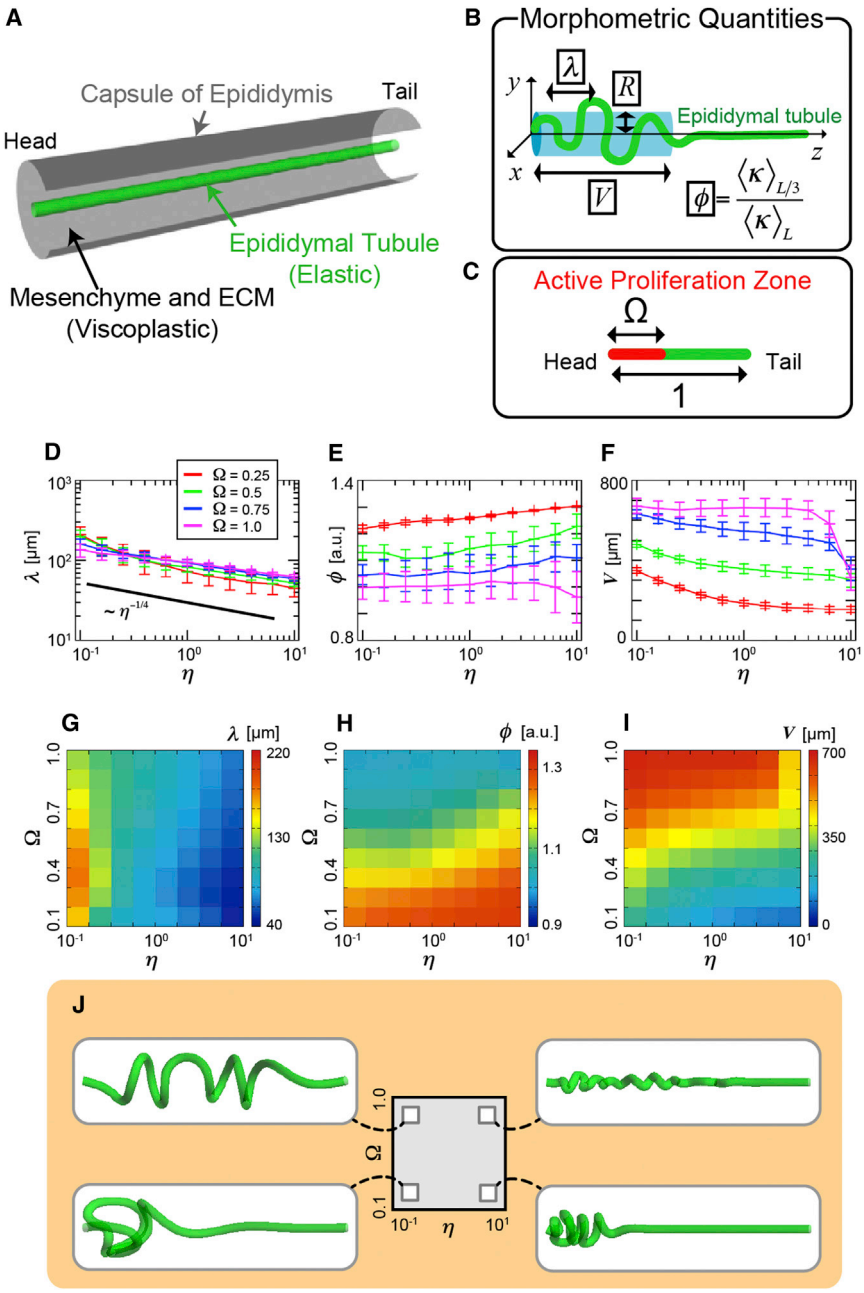

Figure 2. Mathematical Model and Parameter Dependence

(A) Model structure.

(B) The four morphometric quantities λ, ϕ, *V*, and *R*.

(C) Schematics for the index of the active proliferation zone (Ω). Red represents the range in which cell proliferation occurs.

(D–F) The morphometric quantities λ, ϕ, and *V* that represent the change in viscosity of the surrounding tissue (η) and active proliferation zone (Ω). The straight black line in (D) indicates that the result is proportional to $\eta^{-1/4}$. n = 300. The error bars represent the SD.

(G–I) Heatmap of the morphometric quantities for η and Ω. The colors on the graphs represent the mean value in each parameter set, with the red bar indicating large values and blue bar indicating small values. n = 200.

(J) Schematic summary of the numerical analysis. Representative figures are shown at the corner of the parameter space, and the parameter set is one of the combinations of $\eta = 10^{-0.75}$ or $10^{0.75}$ and Ω = 0.25 or 0.75.

analyses under a fixed configuration of the capsule of the epididymis for simplicity. Here, we focus on the changes in two parameters, active proliferation zone (Ω) and viscosity of surrounding tissues (η), and the resulting morphology of the epididymal tubule was evaluated at an early stage of morphogenesis (*t* = 24 hr).

From the numerical analysis, I found that changes in Ω are directly linked to the range over which localized tubule folding occurs (Figures 2E, 2F, 2H, and 2I), whereas the wavelength of the folded tubule is not affected by this range (Figures 2D and 2G). Therefore, the degree of fold localization in the head region decreases according to increases in the area of LECP. This process can be understood intuitively, because the localized folding is a consequence of local tubule deformation driven by LECP.

However, the wavelength of the folded tubule is sensitive to changes in the viscosity of the surrounding tissues (η), with decreasing viscosity resulting in a folded tubule with a longer wavelength (Figures 2D and 2G). This response is roughly consistent with the following analytical expression obtained through scaling arguments (Golubovic et al., 2000) (Figure 2D; Supplemental Experimental Procedures):

$$\lambda \sim \eta^{-1/4}. \qquad \text{(Equation 1)}$$

This relationship clearly indicates that the wavelength of the folded tubule increases monotonically with decreases in the viscosity of the surrounding tissues. Viscosity represents mechanical resistance, and in a viscous environment, the motion of a tubule is relatively suppressed during the process of morphogenesis; therefore, broad-spreading tubule deformation is achieved in less viscous environments and results in a longer wavelength of the folded tubule. Moreover, this analysis suggests that the shape of the tubule should be influenced by changes in viscosity even when the mesenchymal cells surrounding the tubule do not actively exert force on the epididymal tubule.

To summarize the results of the numerical analysis (Figure 2J), I found that the patterning of the folded tubule is primarily determined by Ω and η, and LECP in the head region and appropriate high viscosity in the surrounding tissues are required to achieve localized tubule folding early in morphogenesis.

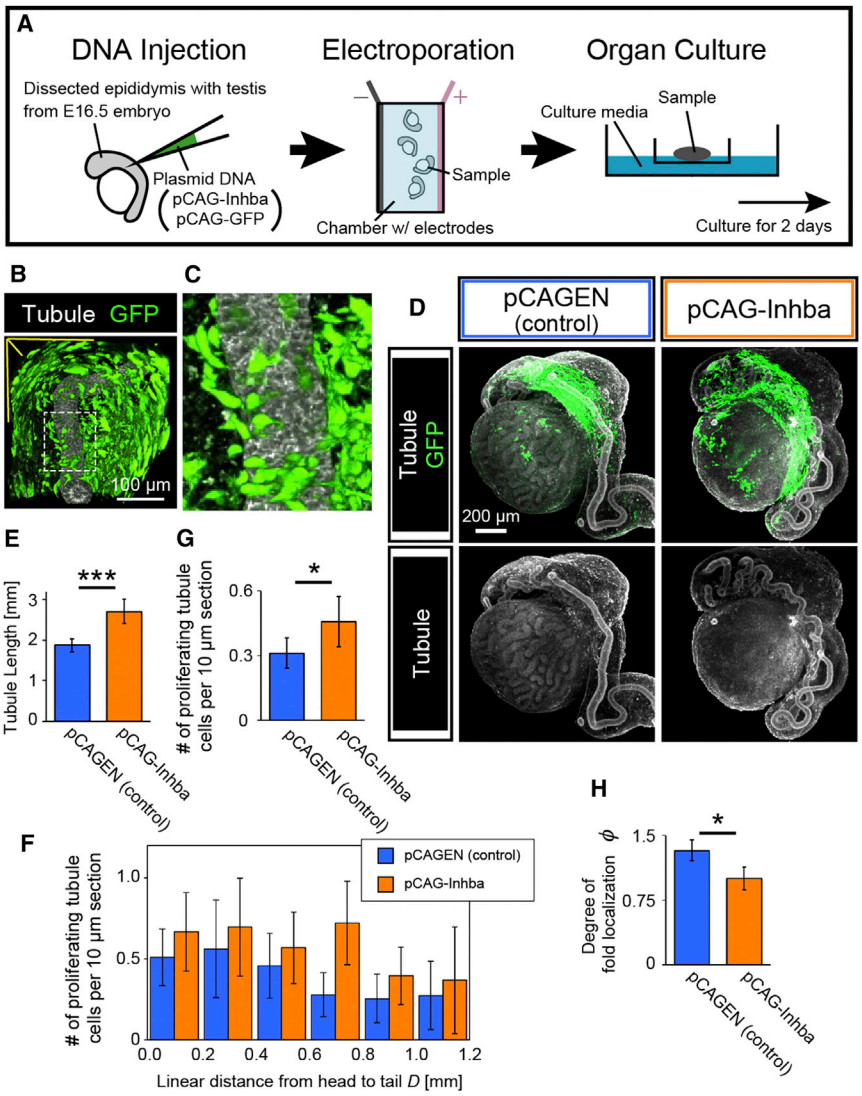

Figure 3. *Inhba* Transfection Assay

(A) Experimental procedures. The plasmid DNA solution contained the pCAG-Inhba and pCAG-GFP vectors as described in the text.

(B) Projection image of 3D stacks of a transfected sample immunostained for E-cadherin (white) and GFP (green).

(C) The magnified image of the dotted square in (B). GFP expression was used as a reporter for the sites of exogenous *Inhba* expression. Scale bar, 100 μm.

(D) Cultured epididymides transfected with the plasmid DNA. The right panel shows an epididymis transfected with pCAG-Inhba, whereas the left panel shows a sample transfected with the control pCAGEN plasmid. Both the tubule morphology and GFP reporter distribution are shown in the upper panels, whereas the tubule morphology is shown in the lower panels for easier observation. Scale bar, 200 μm.

(E) Tubule length for the plasmid transfection. n = 8. $p < 0.01$ (Mann-Whitney U test).

(F) Spatial distribution of pHH3-positive cells in the tubule along the linear distance *D*.

(G) Average number of proliferating cells per 10 μm section throughout the tubule. n = 8 for pCAGEN and n = 6 for pCAG-Inhba. p = 0.042 (Mann-Whitney U test).

(H) Degree of the fold localization (ϕ) for DNA transfection. n = 8. p = 0.026 (Mann-Whitney U test). The error bars represent the SD.

neously injected a CAG-promoter-driven *Inhba* construct using pCAG-GFP as a transfection reporter (Matsuda and Cepko, 2004) into the epididymal tissue at E16.5, which was followed by electroporation of the DNA plasmids according to the procedure shown in Figure 3A. The DNA plasmids were successfully transfected into the mesenchyme surrounding the epididymal tubule (Figures 3B and 3C), and exogenous *Inhba* transcription was induced in the mesenchyme (Figure S3A).

Interestingly, the average number of proliferating cells in the epididymis transfected with pCAG-Inhba was enhanced throughout the tubule along with the alteration of spatial profiles of cell proliferation in the tubule, and the total length of the tubule was elongated compared with the control epididymis (Figures 3D–3G). Moreover, tubule folds were observed in the entire region of the epididymis following transfection with pCAG-Inhba, whereas the tubule folds were localized in the head region in the control (Figure 3H). Note that the tubule diameter and cell shape in the tubule were almost identical between the two treatments (Figures S3B–S3E), suggesting that *Inhba* expression exclusively contributes to the elongation of epididymal tubules in the transfected region. It is apparent that *Inhba*-induced tubule elongation triggered folding throughout the tubule, which corresponds to the model prediction related to the change in Ω in terms of ϕ.

Verification Experiments

To corroborate the model predictions, I performed verification experiments using an in vitro organ culture system in which an epididymis with an attached testis was dissected from an E16.5 embryo and cultured for 2 days. Based on the model analysis, I altered the area of cell proliferation in the epididymal tubule and mechanical resistance of the tissues surrounding the tubule, and I examined the influence of these changes on the tubule shape.

First, I altered the spatial profiles of cell proliferation in the epididymal tubule by introducing DNA constructs into a broad area of the developing epididymis. In an earlier study, it was shown that *Inhba* promotes cell proliferation in the epididymal tubule and a signaling effector of *Inhba* (pSMAD) is active throughout the epididymal tubule; the activity of pSMAD was not detected in the mesenchyme (Tomaszewski et al., 2007). Therefore, inducing *Inhba* expression in the epididymis should induce cell proliferation in the epididymal tubule. Thus, I simulta-

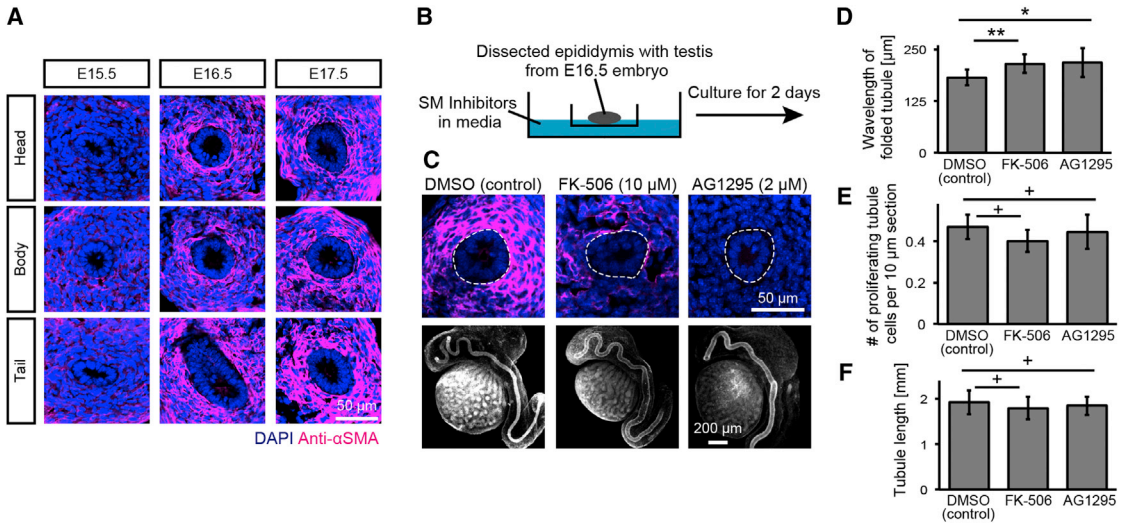

Figure 4. Inhibitor Assay for aSMA Expression

(A) Spatiotemporal distribution of aSMA expression (magenta) together with DAPI staining (blue) in the epididymis. The sections were cut perpendicular to the head-tail axis. Scale bar, 50 μm.

(B) Outline of the experiment.

(C) Changes in the epididymal tubule following treatment with inhibitors. Upper panels show aSMA expression (magenta) and DAPI staining (blue), and lower panels show the morphology of the epididymal tubule immunostained for Pax2. Scale bars, 50 μm for the upper panels and 200 μm for the lower panels.

(D) The wavelength of the folded tubule following inhibitor treatment. n = 11. $p < 0.01$ for DMSO-FK506, and $p = 0.045$ for DMSO-AG1295 (Mann-Whitney U test).

(E) Average number of proliferating cells per 10 μm section throughout the tubule. n = 8. $p = 0.093$ for DMSO-FK506, and $p = 0.297$ for DMSO-AG1295 (Mann-Whitney U test).

(F) Length of the epididymal tubule. n = 11. $p = 0.314$ for DMSO-FK506, and $p = 0.605$ for DMSO-AG1295 (Mann-Whitney U test). The error bars represent the SD.

Next, an experiment was conducted to test the influence of a change in the mechanical resistance of the tissues surrounding the tubule. To alter the mechanical resistance, I selected as a target cell differentiation into smooth muscle, which is known to produce resistance (Hinz, 2010), and found that alpha-smooth muscle actin (aSMA), a marker of smooth muscle differentiation, becomes homogeneously expressed and shows increased levels in the mesenchyme along the head-tail axis beginning at E16.5 and in parallel with the cell rearrangement to enclose the epididymal tubule (Figure 4A). Thus, to block the expression of aSMA, I applied FK-506 and AG1295, which are known inhibitors of aSMA expression, to the culture media (Shyer et al., 2013) (Figure 4B). The suppression of differentiation was expected to lead to a reduction in the passive friction of the surrounding tissue and result in the epididymal tubule exhibiting a longer wavelength, which was predicted in Equation 1.

After 2 days of organ culture with the inhibitors, the expression of aSMA was suppressed in the mesenchyme surrounding the tubule, and the morphology of the epididymal tubule had been altered by these treatments (Figure 4C). The wavelength of the folded tubule became longer following the inhibitor treatments compared with the control, confirming the model prediction (Figure 4D). Although the tubule diameter was slightly increased by the inhibitors, there were no significant differences in either the cell proliferation in the tubule or length of the epididymal tubule between the treatments, indicating that the inhibitors only altered the tubule shape (Figures 4E, 4F, and S4). In conclusion, the experimental results demonstrated that the pattern of a folded epididymal tubule occurs spontaneously as a result of mechanical interactions during the morphogenetic process and is not governed by predetermined specifications in the tubule.

DISCUSSION

In this paper, I have proposed a simple physical mechanism for the formation of a folded epididymal tubule, namely, axial buckling that is caused by compressive forces resulting from cell proliferation in the epididymal tubule. The combination of *Inhba*-induced cell proliferation, which is restricted to the head region, and cell differentiation into smooth muscles around the tubule triggers localized tubule buckling that results in properly folded tubular morphogenesis. I showed that experimental perturbation of the spatial distribution of cell proliferation and changes to the material properties of the tissues surrounding the tubule alter the morphology of the epididymal tubule as predicted by the mathematical model, which indicates that the morphogenetic patterning of the epididymal tubule is not predefined.

There are two remaining unresolved issues related to epididymal tubule morphogenesis that cannot be addressed in the present mathematical model. One is related to the mechanisms responsible for epididymal tubule elongation that occurs while maintaining a constant diameter, i.e., elongation through polarized tubule growth. As previously reported, tubule geometry can be determined by the internal stress in the epithelial tubule that is primarily produced by the orientation of cell

division, with the mitotic spindle orientation in the cells of the tubule tending to be parallel to the longitudinal axis of tubule elongation (Fischer et al., 2006; Tang et al., 2011). In addition to this mechanism, I hypothesize that the external pressure from the tissue surrounding the tubule also contributes to the polarized tubule growth based on my observation that the tubule diameter expands slightly when mesenchymal differentiation into smooth muscle is inhibited (Figure S4). The other issue is related to how the postbending behaviors of the epididymal tubule are controlled. Although the characteristic structure of the epididymal tubule observed from E17.5 onward, which includes the handedness of the tubule torsion and position of the chirality inversions, appears to be stereotypic, such complex tubule shapes are determined stochastically in the present model because the probability distribution provides the positions of the newly added particles that drive tubule deformation. From my perspective, the formation of complex tubule shapes is dependent on the geometry of the tissue, such as the curvature of the tubule in the initial phase of its morphogenesis and surface of the epididymal capsule, and it is also caused by the collective cellular behaviors that are organized from E17.5 onward. To resolve these two issues, a detailed spatiotemporal analysis should be performed to determine the cellular dynamics that result in the tubule morphology and measurements should be conducted of the tissue geometry to ascertain key information. Although it is unlikely that the cell-shape changes and cell recruitment from the mesenchyme contribute to the morphogenesis of the epididymal tubule (Figure 1K) (Hinton et al., 2011), it is worth considering that active cellular movement of the epididymal tubule drives the formation of the complex 3D tubule structure while also maintaining a constant diameter, which should be clarified through a time-lapse imaging analysis of the cellular dynamics during epididymal development.

It may be possible to explain the mechanism of tubular morphogenesis in other internal organs, such as in the kidneys and lungs, based on the buckling instability proposed in this study. For example, during murine kidney development, it has been observed that an epithelial tubule penetrates into the mesenchyme and terminal branching of the epithelial tubule occurs when the tip of the tubule approaches the border of the capsule (Fleury et al., 2006; Unbekandt et al., 2008). These observations allow us to speculate that the growing tubule tip collides with the mesenchyme and ECM that are condensed between the tip and border of the capsule and the epithelial sheet of the tubule tip is deformed via mechanical interactions, i.e., membrane buckling, which contributes to terminal branching as previously proposed (Fleury et al., 2006). However, I am not claiming that buckling-induced patterning is the only mechanism underlying the stereotypic morphogenesis of internal organs, including that of the epididymis. Consecutive events occur at the molecular and cellular level through biomechanical and biochemical interactions that presumably drive the robust morphogenetic processes of tubular patterning and result in the emergence of stable functional structures in internal organs (Varner and Nelson, 2014). I believe that continued investigations of both aspects will lead to further discoveries regarding the general principles of organogenesis.

EXPERIMENTAL PROCEDURES

Statistical Analysis

Statistical analyses were performed with the free software R. p values < 0.05 were considered to be statistically significant. The range of p values is represented in the graph as follows: +p > 0.05, *p < 0.05, **p < 0.005, ***p < 0.0005. The statistical tests applied in the analysis are described in the figure legends.

DNA Transfection via Electroporation

For the construction of pCAG-Inhba, cDNA encoding mouse *Inhba* was amplified via PCR, including the 5′ and 3′ UTRs (PCR primers: 5′-GGGG TTCGCTAGTGGCTGCTC-3′ and 5′-CATTTTGCCACTGTCTTCTCTGGAC-3′) and cloned into the pCAGEN vector (Matsuda and Cepko, 2004; Niwa et al., 1991) with multiple cloning sites. Mixed DNA solutions of the pCAG-Inhba and pCAG-GFP vectors (1 μg/μl each) in PBS were injected into the dissected epididymides of E16.5 embryos through a fine glass capillary tube under a dissecting microscope. The volume of injected DNA was less than 0.5 μl. After DNA injection, the epididymides with testes were transferred to a microelectroporation chamber (CUY520P5, Nepagene) that was filled with PBS. A NEPA21 Super Electroporator (Nepagene) was used for electroporation. Three 10 ms square pulses (150 V) with a 10% decay rate at intervals of 50 ms were applied as transfer pulses, which were followed by five 50 ms square pulses (10 V) with a 40% decay rate at intervals of 50 ms as poring pulses.

SUPPLEMENTAL INFORMATION

Supplemental Information includes Supplemental Experimental Procedures, four figures, two tables, and three movies and can be found with this article online at http://dx.doi.org/10.1016/j.celrep.2014.09.041.

ACKNOWLEDGMENTS

This work was supported by the Japan Society for the Promotion of Science (JSPS) KAKENHI grant 12J03338. Part of this work was supported by the Platform for Dynamic Approaches to Living Systems of the Ministry of Education, Culture, Sports, Science and Technology of Japan and by a Grant for Basic Science Research Projects from the Sumitomo Foundation. I would like to thank H. Wada of Ritsumeikan University and J. Silverberg of Cornel University for their very helpful comments regarding the section on mathematical modeling, H. Shimojo and T. Matsuda of Kyoto University for their technical advice on the experiments, T. Matsuda for kindly providing the pCAGEN vector, and S. Hayashi of RIKEN CDB and R. Kageyama of Kyoto University for general discussions.

Received: May 23, 2014
Revised: August 22, 2014
Accepted: September 22, 2014
Published: October 23, 2014

REFERENCES

Ball, E.M., and Risbridger, G.P. (2001). Activins as regulators of branching morphogenesis. Dev. Biol. *238*, 1–12.

Dong, B., Hannezo, E., and Hayashi, S. (2014). Balance between apical membrane growth and luminal matrix resistance determines epithelial tubule shape. Cell Rep. *7*, 941–950.

Fischer, E., Legue, E., Doyen, A., Nato, F., Nicolas, J.-F., Torres, V., Yaniv, M., and Pontoglio, M. (2006). Defective planar cell polarity in polycystic kidney disease. Nat. Genet. *38*, 21–23.

Fleury, V., Watanabe, T., Nguyen, T.H., and Unbekandt, M. (2006). Physical mechanisms of branching morphogenesis in animals. In Branching Morphogenesis, J.A. Davis, ed. (New York: Springer), pp. 202–234.

Golubovic, L., Moldovan, D., and Peredera, A. (2000). Flexible polymers and thin rods far from equilibrium: buckling dynamics. Phys. Rev. E Stat. Phys. Plasmas Fluids Relat. Interdiscip. Topics *61*, 1703–1715.

Hinton, B.T., Galdamez, M.M., Sutherland, A., Bomgardner, D., Xu, B., Abdel-Fattah, R., and Yang, L. (2011). How do you get six meters of epididymis inside a human scrotum? J. Androl. *32*, 558–564.

Hinz, B. (2010). The myofibroblast: paradigm for a mechanically active cell. J. Biomech. *43*, 146–155.

Joseph, A., Yao, H., and Hinton, B.T. (2009). Development and morphogenesis of the Wolffian/epididymal duct, more twists and turns. Dev. Biol. *325*, 6–14.

Matsuda, T., and Cepko, C.L. (2004). Electroporation and RNA interference in the rodent retina in vivo and in vitro. Proc. Natl. Acad. Sci. USA *101*, 16–22.

Metzger, R.J., Klein, O.D., Martin, G.R., and Krasnow, M.A. (2008). The branching programme of mouse lung development. Nature *453*, 745–750.

Niwa, H., Yamamura, K., and Miyazaki, J. (1991). Efficient selection for high-expression transfectants with a novel eukaryotic vector. Gene *108*, 193–199.

Robaire, B., Hinton, B.T., and Orgebin-Crist, M.-C. (2006). The epididymis. In Knobil and Neill's Physiology of Reproduction, Third Edition, J.D. Neill, ed. (New York: Academic Press), pp. 1071–1148.

Savin, T., Kurpios, N.A., Shyer, A.E., Florescu, P., Liang, H., Mahadevan, L., and Tabin, C.J. (2011). On the growth and form of the gut. Nature *476*, 57–62.

Shyer, A.E., Tallinen, T., Nerurkar, N.L., Wei, Z., Gil, E.S., Kaplan, D.L., Tabin, C.J., and Mahadevan, L. (2013). Villification: how the gut gets its villi. Science *342*, 212–218.

Tang, N., Marshall, W.F., McMahon, M., Metzger, R.J., and Martin, G.R. (2011). Control of mitotic spindle angle by the RAS-regulated ERK1/2 pathway determines lung tube shape. Science *333*, 342–345.

Tomaszewski, J., Joseph, A., Archambeault, D., and Yao, H.H. (2007). Essential roles of inhibin beta A in mouse epididymal coiling. Proc. Natl. Acad. Sci. USA *104*, 11322–11327.

Unbekandt, M., del Moral, P.M., Sala, F.G., Bellusci, S., Warburton, D., and Fleury, V. (2008). Tracheal occlusion increases the rate of epithelial branching of embryonic mouse lung via the FGF10-FGFR2b-Sprouty2 pathway. Mech. Dev. *125*, 314–324.

Varner, V.D., and Nelson, C.M. (2014). Cellular and physical mechanisms of branching morphogenesis. Development *141*, 2750–2759.

Wada, H., and Netz, R.R. (2009). Hydrodynamics of helical-shaped bacterial motility. Phys. Rev. E Stat. Nonlin. Soft Matter Phys. *80*, 021921.